PAPER
Raoul Naumann d'Alnoncourt *et al.*
Tuning catalysis by surface-deposition of elements on
oxidation catalysts *via* atomic layer deposition

PAPER

Tuning catalysis by surface-deposition of elements on oxidation catalysts *via* atomic layer deposition†

Frederik Rüther, [iD] [a] Robert Baumgarten, [iD] [a] Fabian Ebert, [a] Esteban Gioria, [iD] [a] Raoul Naumann d'Alnoncourt, [iD] *[a] Annette Trunschke [iD] [b] and Frank Rosowski [ac]

Based on the concept that most reaction steps proceed only at the surface layer of a bulk catalyst, the catalytic impact of the surface-modification with PO_x, BO_x, and MnO_x in the selective oxidation of ethane, propane, and *n*-butane is systematically studied. Three different promoter elements are deposited as a sub-monolayer on the surface of oxidation catalysts with high dispersion by sequential and self-limiting reactions at the solid–gas interface, using atomic layer deposition. Oxygenate and olefin selectivities are tuned by the surface deposition of PO_x and BO_x, leading to improved product yields. The mixed metal oxide $MoVTeNbO_x$ is used as a case study to demonstrate the effect of the modification in different reactions with yield improvements of up to 24% in the propane oxidation towards acrylic acid. It is shown that the beneficial performance is related to a change in surface composition, a modification in the electronic properties of the redox active element vanadium, and a decrease in acidity. A comparative study considering several bulk catalysts and deposited elements revealed further promoting effects for different oxidation catalysts. In particular, the deposition of PO_x on V-containing oxides suppresses CO_x formation. Precisely adjusted surface modifications leading to enhanced product yields demonstrate the potential of atomic layer deposition as a powerful tool for tuning catalytic properties of bulk catalysts.

Introduction

On the way towards a greener chemical industry existing processes must be optimized, which depends strongly on advances in heterogeneous catalysis.[1–3] Every chemical conversion step is accompanied by a loss in resources and energy. The goal of sustainability can only be achieved by minimizing this loss, either by reducing the overall number of transformations or tuning overall product yields. Partial oxidations of light alkanes have been studied for decades as promising reaction routes converting feedstocks directly into valuable chemicals.[4] Preventing consecutive and parallel reactions, leading to the formation of combustion products, is still a difficult task. However, in the case of highly optimized selective oxidation reactions like the *n*-butane (C_4) oxidation to maleic anhydride (MAN) on vanadyl(IV) pyrophosphate (VPP)[5–9] or the direct oxidation of propane (C_3) to acrylic acid (AA) using $MoVTeNbO_x$,[10–12] two promising

catalysts were identified.[5,13] The oxidative dehydrogenation (ODH) of ethane (C_2) is a prospective reaction route for the on-demand production of ethylene using similar catalysts.[14,15] One of the main challenges in understanding the underlying catalytic principles is the dynamic behaviour and self-adapting nature of the catalysts under reaction conditions.[16–19] In literature, this phenomenon is described as 'flexible surfaces', where the chemical potential of the gas phase affects the surface state and changes the surface composition of the bulk catalyst.[20–23] However, structural changes are actually proceeding only at the surface itself or within a thin subsurface layer (0.5–1 nm determined for VPP[24] or $MoVTeNbO_x$[18]), while the bulk functions *e.g.* as an electron or oxygen carrier.[20,25]

In situ characterization revealed a shift in the oxidation state of the redox active element vanadium(V) on the surface of VPP.[17,26–28] While it is fixed to V^{4+} based on the stoichiometry of the bulk, the detection of V^{5+}-species supports the hypothesis that the actual active phase of a catalyst can be very different from the bulk.[8,29–32] Similarly, the crucial influence of the gas phase is studied for $MoVTeNbO_x$.[13,18,33,34] The active and selective surface layer is formed under reaction conditions with a strong influence of added steam, inducing an enrichment of V^{5+} and depletion of Mo^{6+} sites.[12,19,20,35,36] Recently, a data driven approach[37] was applied to a clean catalytic data set with the goal to

[a] BasCat - UniCat BASF JointLab, Technische Universität Berlin, D-10623 Berlin, Germany. E-mail: r.naumann@bascat.tu-berlin.de

[b] Department of Inorganic Chemistry, Fritz Haber Institute of the Max Planck Society, D-14195 Berlin, Germany

[c] Catalysis Research, BASF SE, D-67065 Ludwigshafen, Germany

† Electronic supplementary information (ESI) available: Further experimentation, details on experiments and characterisation (PDF) and complete catalytic data set (XLSX). See DOI: https://doi.org/10.1039/d2cy02184f

This journal is © The Royal Society of Chemistry 2023

Catal. Sci. Technol., 2023, **13**, 4117–4130 | **4117**

connect the materials properties and underlying physical principles to the performance of different catalysts in selective oxidations.[38,39] The targeted reduction of total oxidation can be related to surface composition, surface area, redox activity, and isolation of active sites responsible for the formation of olefins (C_2, C_3). With oxygenates as the target product (C_4, C_3) the electronic properties of the bulk and the surface, as well as the adsorption properties of the catalyst are crucial.[40]

Hence, the catalytic functionality of bulk catalysts is determined by the properties of the termination layer, which depends on the bulk composition and is formed under reaction conditions.[24,26,36,41–43] However, the surface can additionally be modified using synthetic methods like atomic layer deposition (ALD). The deposition of elements *via* volatile precursors using self-limiting surface reactions during ALD is utilized to tune the properties of the catalyst precursor at the atomic level.[44–50] Most commonly it is used for surface decoration or promotion of bulk catalysts[51–53] or advanced catalyst synthesis.[54–56] Here, ALD provides a high dispersion of the deposited elements, to improve activity, selectivity, or stability. Additionally, ALD has the advantage of a solvent-free deposition of promotors, so that the mechanical properties of the bulk catalyst are sustained. This enables to elucidate on reaction mechanisms or property performance relationships.[52]

This work features the surface modification of oxidation catalysts to optimize catalytic (surface-)properties. First, the catalytic functionality of six different oxidation catalysts and their potential to selectively activate alkanes is discussed. Then, oxides (PO_x, BO_x, MnO_x) with potentially promoting effects are deposited on the catalyst surface in sub-monolayers using ALD and the catalytic impact is studied in the selective oxidation of ethane, propane, and *n*-butane. As the deposition of PO_x on V_2O_5 showed promising results in *n*-butane oxidation,[51,52] this concept is transferred to reactions of propane and ethane and more selective oxidation catalysts. The mixed metal oxide $MoVTeNbO_x$ is tuned by the deposition of PO_x and BO_x, leading to improved product yields. With this study we demonstrate

that ALD is as a versatile tool to promote oxidation catalysts, while the basic catalytic features of the host structures are maintained.

Results and discussion

Comparative functionality analysis of base catalysts

A collection of six oxide and phosphate catalysts were selected for their broad range in catalytic behaviour and studied in the oxidation of ethane, propane, and *n*-butane. From a variety of elements, V or Mo-based materials show the most promising performance in selective oxidations. However, binary or monometallic oxides V_2O_5[51,57] or MoO_3[58,59] show either a very low alkane conversion or product selectivity. In contrast, the combination of these elements, preferably with more complex structural features, *e.g.* $MoVO_x$ with M1-structure type,[60–62] have a much higher capability to selectively oxidize the reactant. By introducing Te and Nb into the M1 structure, $MoVTeNbO_x$ was obtained as an excellent catalyst for the oxidative dehydrogenation of ethane (ODHE) and the direct oxidation of propane to AA.[15,63–65] For an efficient oxidation of *n*-butane to MAN, vanadium phosphate (VPO) catalysts or more specifically VPP, are industrially applied.[9,66] As an alternative for V, as redox active element, Mn is studied for the activation of light alkanes. Here, the perovskite structured $SmMnO_3$ is included, which was applied in the oxidative dehydrogenation of propane[67,68] (see Fig. SI1† for XRPD patterns of all catalysts). While these catalysts were mostly studied in literature in one specific reaction, a comparative study under different reaction feeds is way less prominent.[63,69] The functionalization of different alkanes (see desired reaction pathways eqn (1)–(3)) follows very similar steps, namely the activation of a C–H bond, the abstraction of two hydrogen atoms and, in case an oxygenate is formed, the insertion of oxygen into the molecule. Also, in all three reactions the water formation as couple-product is an important driving force.[42] However, for each reaction a different amount of electron transfers needs to be performed and the amount of side products increases with the alkane chain-length.
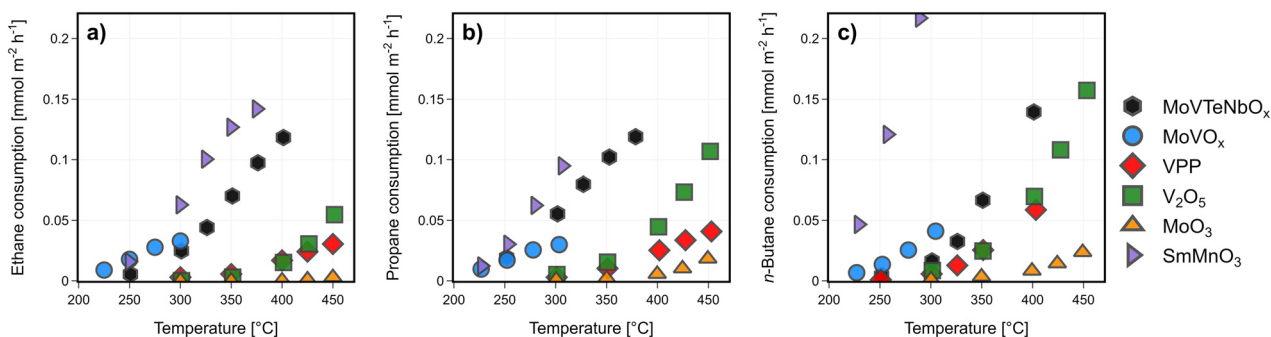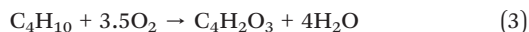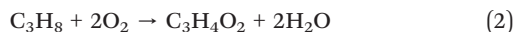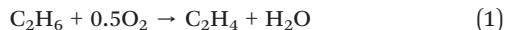

Fig. 1 Catalytic activity of $MoVTeNbO_x$. $MoVO_x$, MoO_3, V_2O_5, VPP and $SmMnO_3$: alkane consumption rates normalized to the surface area [mmol m^{-2} h^{-1}] as a function of the reaction temperature in (a) ethane, (b) propane, and (c) *n*-butane oxidation; the corresponding alkane conversions and consumption rates normalized to weight can be found in Fig. SI3;† oxygen consumption rates are shown in Fig. SI4;† $C_2H_6/O_2/H_2O$ = 3/9/0 % vol, $C_3H_8/O_2/H_2O$ = 3/9/20 % vol, $C_4H_{10}/O_2/H_2O$ = 2/20/3 % vol, 1 atm, 1000 h^{-1} (C_2, C_3)/2000 h^{-1} (C_4).

$$C_2H_6 + 0.5O_2 \rightarrow C_2H_4 + H_2O \qquad (1)$$

$$C_3H_8 + 2O_2 \rightarrow C_3H_4O_2 + 2H_2O \qquad (2)$$

$$C_4H_{10} + 3.5O_2 \rightarrow C_4H_2O_3 + 4H_2O \qquad (3)$$

Catalytic activity is a function of multiple parameters with the surface area as one important factor, which varies for the studied catalysts between 3 m^2 g^{-1} (MoO_3) and 36 m^2 g^{-1} ($MoVO_x$). Therefore, Fig. 1 shows a comparison in the catalytic activity using the alkane consumption rates normalized to the surface area (see Table SI1 and Fig. SI2† for details on the N_2-physisorption). The perovskite catalyst $SmMnO_3$ shows the highest alkane consumption rate in all three reactions. $MoVO_x$ shows a similar alkane conversion level at low temperatures, as 300 °C is the maximum temperature to avoid full conversion (see alkane conversion in Fig. SI3†) and catalyst decomposition, but the consumption rate is either slightly higher or similar to the other catalysts. In contrast, V_2O_5 and VPP show an intermediate activity, while the alkane consumption rates gradually decrease with the reduction in alkane chain-length and are therefore following the energetics to activate the different C–H bonds.[70] Interestingly, the mixed metal oxide $MoVTeNbO_x$ shows a high alkane consumption in all three reactions, which seems to be rather independent of the chain-length of the reactant. This also applies to $MoVO_x$. The rate of alkane consumption on MoO_3 is very low. For the V-containing compounds, the beneficial effect of V as active element in the C–H activation can be observed, while it is even surpassed by manganese incorporated into the perovskite structure of $SmMnO_3$. In addition, the combination of different elements seems to promote the catalytic activity, as much lower temperatures are necessary to achieve high reaction rates.

In general, the rate of alkanes consumption is not only a function of C–H activation. Fig. 2 shows the product distribution obtained with the catalysts normalized to a fixed alkane conversion level. The formation of the various products requires additional centres for C–C bond cleavage or oxygen insertion. In the case of propane and n-butane, oxygenates are formed in much higher selectivity on the catalysts surface compared to ethane oxidation (see Fig. 2 and contact time variation study in Fig. SI5 and SI6†). Therefore, the reaction rate is not only determined by the alkane activation, as the constant rates on $MoVTeNbO_x$ and $MoVO_x$ suggest. A re-adsorption of already formed products also might play a role.

In all three reactions, the perovskite $SmMnO_3$ produces CO_2 as the main product. As a minor product the respective olefin is formed. V_2O_5 mostly generates CO_2 from ethane, while CO is formed as main product from propane and n-butane. Also, in C_4-oxidation MAN and acetic acid can be detected as reaction products, especially at a low conversion level. MoO_3 shows a similar product distribution, while the overall alkane conversion is very low (<5%). $MoVTeNbO_x$, $MoVO_x$, and VPP are by far the most selective catalysts. While
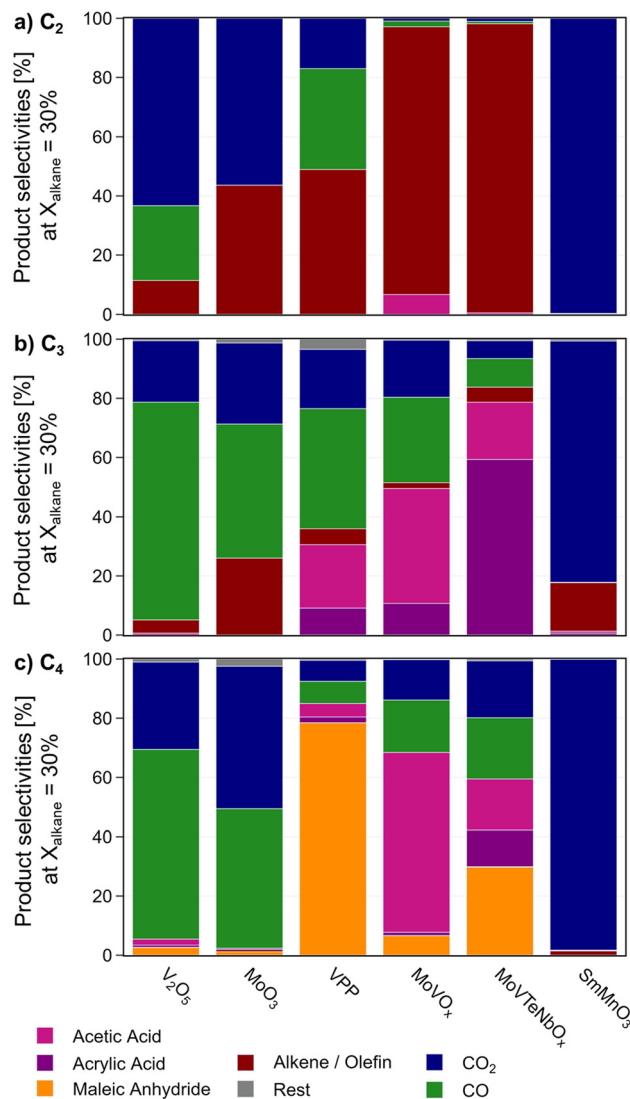

Fig. 2 Product selectivity in a) ethane, b) propane, and c) n-butane oxidation, interpolated to a fixed alkane conversion of X_{alkane} = 30% during the temperature variation study; in case of MoO_3 the maximum temperature setpoint of 450 °C is used, due to overall low conversions X_{alkane} < 30%; $C_2H_6/O_2/H_2O$ = 3/9/0 % vol, $C_3H_8/O_2/H_2O$ = 3/9/20 % vol, $C_4H_{10}/O_2/H_2O$ = 2/20/3 % vol, 1 atm, 1000 h^{-1} (C_2, C_3)/2000 h^{-1} (C_4).

VPP suffers from consecutive oxidation of the desired products in C_3 and C_2 oxidation (see contact time variation study in Fig. SI6†), it shows the maximal yield towards MAN from n-butane. The mixed metal oxides are more prone to break the C–C bond in this reaction leading to the formation of lower oxygenates like acrylic and acetic acid. On the other hand, higher oxygenate selectivity is achieved by the oxide catalysts from propane with $MoVTeNbO_x$ producing AA as main product. Based on a comparison between the consumption rate of the alkane and oxygen (see Fig. SI4†), the superior performance of $MoVTeNbO_x$ in ODHE and C_3-oxidation is related to a comparably low oxygen consumption at high alkane conversion levels. In comparison, $MoVO_x$ is more active in C–C bond splitting and forms lower oxygenates
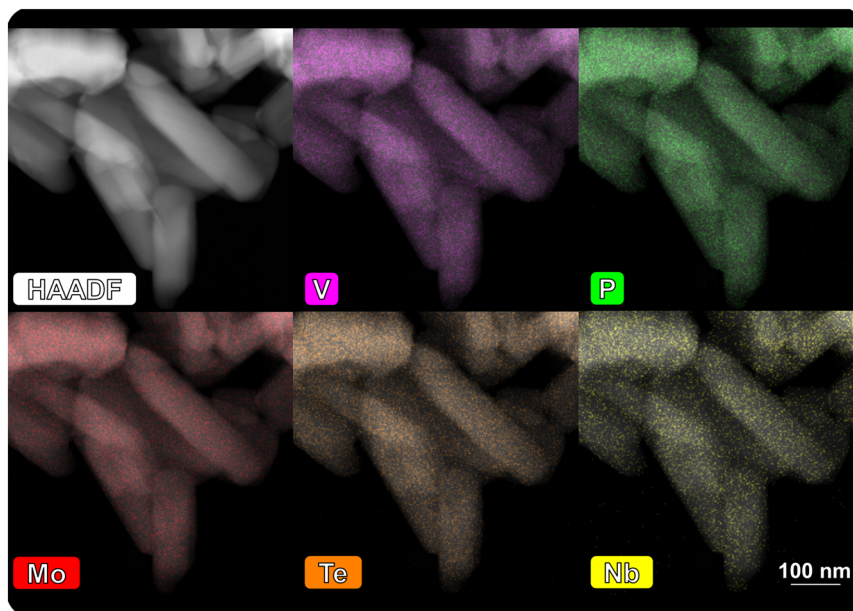
This journal is © The Royal Society of Chemistry 2023

Catal. Sci. Technol., 2023, **13**, 4117–4130 | **4119**

Fig. 3 STEM-HAADF images of PO_x surface-modified $MoVTeNbO_x$ after catalysis (spent sample): EDX-mappings show element dispersion of both bulk elements (Mo, V, Te, Nb) and the additionally deposited phosphorus; the images of the fresh sample are shown in Fig. SI8,† the mapping-spectra of both samples are attached in Fig. SI9 and SI10.†

from the feedstock. The oxidative dehydrogenation of ethane proceeds very selectively on both mixed metal oxides with M1 structure, while the formation of small amounts of acetic acid can only be attributed to $MoVO_x$.

The studied catalysts clearly differ in the capability to activate the different alkanes, based on the change in performance (see Fig. 1). The apparent activation energies of both reactants (ethane, propane, or n-butane, and oxygen) are plotted to compare the potential of the respective catalyst to partially oxidize the feedstock (yield 1-CO_x), visualized in Fig. SI7.† In case of oxidative dehydrogenation of ethane, the highest ethylene selectivity is measured for medium apparent activation energies. In case of $SmMnO_3$ apparent activation energies are very low, which corresponds to the high ethane consumption rate with CO_2 as main product. The low capability of V_2O_5 to activate ethane is clearly visible, indicated by very high activation barriers. The samples producing ethylene in medium (VPP) or even high yields ($MoVTeNbO_x$, $MoVO_x$) show both an intermediate apparent activation energy of the alkane and the gas phase oxygen, which is assumed to mostly act to re-oxidize the oxygen vacancy of the bulk following the Mars–van Krevelen mechanism.[26,71,72] Compared to the oxidative dehydrogenation, the selective oxidation of propane and n-butane forming oxygenates is more complex. Therefore, the trends between the alkane activation and the product yield are not following linear relationships (C_3, C_4), as multiple reaction pathways are proceeding in parallel. As a result, certainly different catalytic properties are required to either proceed the initial dehydrogenation step of the alkane forming olefins than the consecutive oxidation towards oxygenates like AA or MAN.[40] In general, the measured

apparent activation energies with the respect to the oxygen consumption rate for all catalysts depend on the alkane, which clearly shows that the chemical potential of the gas phase has an impact on the surface composition, defect concentration, and the electronic properties of the catalysts.

Surface modification by deposition of elements *via* ALD

Based on the functionality analysis of the bulk catalysts in the literature and in the present work, it is found that the combination of different elements within a phosphate or oxide structure is favourable for catalysis (*e.g.* the incorporation of Nb and Te into a Mo–V oxide structure[73]). Accordingly, the six base catalysts are modified by three different promoting elements, namely phosphorus, boron and manganese, introduced to the surface, ultimately as oxides (details can be found in the Experimental section). Within the entire periodic table, a large number of elements have been identified in the past that are active or beneficial in catalytic conversion of hydrocarbons.[74] Many elements have already been deposited on oxides by ALD, but only a minority of the materials thus prepared have been studied in catalysis.[50] Phosphates are discussed to play a crucial role in the oxidation of n-butane.[47,52,75] While most of the redox steps are attributed to the V, phosphorus itself or the ratio between V and P is often discussed as one important factor for a selective oxidation of the alkane.[5,75–78] Additionally, P has a positive effect as doping element in mixed metal oxide catalysts and P–Mo–V compounds were found to selectively oxidize isobutane.[79,80] It was proposed that additional acidic properties correlate with increased performance. Similarly, boron is discussed to promote the partial oxidation of alkanes.[81,82] Bulk boron

containing catalysts are discussed to be highly selective in oxidative dehydrogenation reactions *e.g.* of propane.[83] Surface-stabilized BO_x species are proposed as active site,[84,85] although it has been shown that the function of the boron oxide can at most be the initiation of radical chain reactions in the gas phase.[81,86–88] While P mostly shows promoting effects in combination with a transition metal, the deposition of Mn introduces another redox active element on the surface of the catalysts. Mn-Tungstates are among the rare cases of V-free oxidation catalysts for the dehydrogenation of propane to propylene.[89] In summary, it can be expected that Mn introduced to the system predominantly contributes to the activity, while P promotes selectivity. Added surface sites of BO_x potentially accelerate the dehydrogenation of the alkanes leading to higher product yields.

The impact of the surface modification on the surface properties and the catalytic performance is discussed exemplary for $MoVTeNbO_x$, as it shows unique performance in the selective oxidation of C_2, C_3 and C_4. The deposition of the element precursors, the subsequent treatment (ligand-removal under O_2 or H_2O feed diluted with N_2) and the final calcination of the modified catalyst maintain the structural integrity of the bulk. Comparison of the XRPD patterns (Fig. SI11†) and N_2-physisorption measurements (Fig. SI12†) before and after the modification confirms that no additional phases are formed and that the morphology, the specific surface area, and the pore volume remain constant (see Table SI2†). The amount of deposited PO_x, BO_x and MnO_x is quantified by the overall mass gain throughout the surface deposition (*e.g.*, Δw = +1.8 wt% of PO_x on $MoVTeNbO_x$, see Fig. SI13†). Additionally, ICP-OES is used to analyse the overall element loading. With regard to the total catalyst mass, it is found that only 0.9 wt% (B) or 0.8 wt% (P) are deposited (Table SI4†). The deviation between the quantification methods is related to the introduction of the additive as oxide species to the surface, adding weight in the balance. The modified surface composition and therefore the amount of the deposited ALD-element is determined by the properties of both, the base catalyst (*e.g.*, OH-group density, surface area) and the utilized ALD-precursor (reactivity, ligand-molecule size) and therefore varies between the modified samples. A homogeneous dispersion is confirmed by STEM-EDX mapping of PO_x on $MoVTeNbO_x$ (Fig. 3). Moreover, the dispersion of PO_x on $MoVTeNbO_x$ can be maintained during the reaction in propane oxidation under the rather harsh conditions (c_{Steam} = 20%), as the mappings of the spent catalyst indicate.

In contrast to the bulk characteristics, the introduction of the elements shows a significant effect on the near-surface properties. In order to describe these changes in detail, the chemical state of the samples at the near-surface is investigated by XPS (details can be found in the Experimental section). Fig. 4a illustrates the variation in composition of near-surface elements by the deposition of BO_x, PO_x and MnO_x on $MoVTeNbO_x$. Interestingly, the addition of a fifth element does not always lead to a similar change in the surface concentrations of the bulk elements. While the
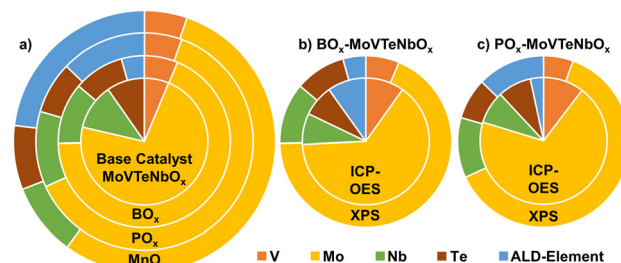

Fig. 4 (a) Impact on near-surface composition (at%), while excluding the oxygen content, by surface modification (BO_x, PO_x, MnO_x) of the $MoVTeNbO_x$ catalyst before catalysis determined by XPS measurements; comparison between near-surface (XPS) and overall bulk (ICP-OES) composition of (b) BO_x-modified and (c) PO_x-modified $MoVTeNbO_x$. The raw data of the measurements is summed up in Tables SI3 and SI4† and the composition of the spent samples is visualized in Fig. SI14 and SI15.†

deposition of Mn lowers the amount of the other elements evenly, the addition of BO_x shows specifically a depletion of Mo^{6+} on the surface and, at the same time, a slight increase in V availability. Furthermore, the combination of ICP-OES and XPS measurements is used to specify the location of the elements after calcination. Therefore, the B seems to migrate directly into the bulk of the catalyst, as a higher content of B can be detected in the bulk (ICP-OES) compared to the near-surface (XPS, see Fig. 4b). In contrast PO_x is enriched on the surface (Fig. 4c).

Tuning surface properties of oxidation catalysts

The deposition of additional elements on the catalysts results in a modification of the near-surface composition, with respect to the added ALD-elements, but also with respect to the original bulk elements. To elaborate further on this effect, the chemical state of the (redox active) elements at the near-surface is studied by XPS. While most of the transition metals only show one specific oxidation state in the spectra (Mo^{6+}, Nb^{5+}, Te^{4+}), which is maintained during the modification, a change in the average oxidation state of V is observed, presented after catalysis in Fig. 5. In all $MoVTeNbO_x$-samples surface-species with two different oxidation states (V^{4+} and V^{5+}) are detected (XPS spectra can be found in Fig. SI16†). To characterize a more oxidized or reduced overall surface state, the ratio R_{XPS} between V^{4+} and the sum of V^{4+} and V^{5+} is calculated (see Experimental section for details). The unmodified $MoVTeNbO_x$ shows a slightly reduced surface state with more V^{4+} present at the surface. The deposition of the elements by ALD leads to a change in the oxidation state of the redox active element after catalysis. While the Mn modified sample shows an even more reduced surface state with respect to V, the PO_x- and BO_x-modified surfaces show a higher average oxidation state of V. An enrichment of V^{4+} or V^{5+} at the surface is often correlated to catalytic performance based on both *in situ* and *ex situ* analytics in case of $MoVTeNbO_x$.[12,34,59] In a previous work, Knemeyer *et al.* show that the deposition of a phosphorus
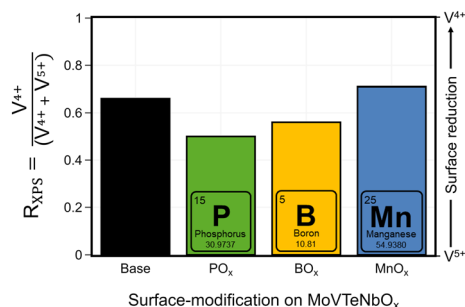
This journal is © The Royal Society of Chemistry 2023

Catal. Sci. Technol., 2023, **13**, 4117–4130 | **4121**

Fig. 5 Effect of surface deposition of BO_x, PO_x, MnO_x on the oxidation state of V in the near-surface region of $MoVTeNbO_x$ after catalysis (spent); the ratio R_{XPS} between reduced V^{4+} species and the sum of V^{4+} and V^{5+} calculated from the XPS spectra in the of V $2p_{3/2}$ region (see Fig. SI16 and SI17† for more details) is shown.

precursor has the potential to reduce surface V^{5+} to V^{4+} starting from a V_2O_5, which mostly contains V^{5+} in its bulk structure and at the surface.[52] However, the calcination of the sample in the second ALD half-cycle (PO_x on V_2O_5), resulted in a re-oxidation of the V-species at the surface. In the present case of $MoVTeNbO_x$, the decoration with PO_x and BO_x induces an oxidized surface state after catalyst testing.

In addition to the electronic properties of the redox-active element V, the selectivity of heterogeneous catalysts in oxidation reactions is determined by multiple phenomena, that need to collaborate to activate adsorbed reactants and convert them into the desired product. Many of these processes are strongly influenced by the interaction between the surface elements and the gas phase molecules. As a result, the surface-acidity of a catalyst often correlates with performance.[90–93] Acidity can contribute to the C–H activation,[94] while strong acid sites can lower the product selectivity by undesired parallel or consecutive reactions.[92] As a result, the acidity of mixed metal oxides and especially of Mo and V based catalysts are studied in much detail in literature with the goal to correlate it with the performance in partial oxidation reactions.[69,73,95–97]

While both Brønsted and Lewis acid sites are discussed to play a role in catalysis, their presence is also crucial for the described deposition of atomic layers on the oxide surface. During ALD, the element precursors are interacting e.g. with surface hydroxyl-groups, which can exhibit Brønsted acidity, and thus chemisorb onto the surface.[50,53] After the surface is saturated with the precursor, in a second step using O_2 or H_2O new hydroxyl groups both on the deposited elements and bulk-species are created. The determination of the surface acidity is complicated, as multiple surface properties of a heterogeneous catalyst are mutually depending on each other (e.g. oxidation state or redox activity and acidity[93]). In this work, NH_3-pulse studies are used as a tool to describe the impact on the surface characteristics by the surface deposition of different elements. NH_3-desorption experiments at temperatures above the calcination temperature of the catalysts can lead to an undesired formation of gaseous species other than ammonia, which impedes correct

quantification of desorbed ammonia. PO_x introduced to the surface of $MoVTeNbO_x$ by ALD clearly decreases the overall amount of adsorbed ammonia, while for BO_x a slight reduction can be observed, which indicates a lower availability of acidic sites on the surface of the modified catalysts, as shown in Fig. 6. The lower acidity is in line with the composition change on the surface of the catalyst, as the boron mostly migrates to the bulk of the catalysts (see Fig. 4). Although the overall amount of deposited BO_x surpasses the deposition of PO_x (ICP-OES), on the surface of the modified catalysts the opposite effect can be observed, with more PO_x accumulated at the surface (see Tables SI3 and SI4†). This is an indicator why the PO_x-deposition has a more pronounced effect on the surface properties like the acidity. However, the addition of P and B is discussed to add acidic features as dopants,[79] increased P-content in Mo-phosphate lead to higher acidity,[98] and surface P–OH groups were shown to contribute to the Brønsted-acidity in VPP.[99] On the contrary, in case of supported alumina[100] or zeolite[101] catalysts, the addition of phosphates was utilized to reduce acidity. In this study, the deposition of the surface groups has two effects. First, surface OH-groups are exchanged and saturated by the added ALD-groups. This introduces additional sites, where ammonia can adsorb, but also potentially blocks acid sites of the base catalysts. A similar decrease in adsorbed NH_3 or acidity of the catalyst was observed for doping experiments of $MoVTeNbO_x$ with Bi, leading to improved performance in the synthesis of acrylonitrile.[102] The sample modified by MnO_x shows that the surface treatment can also result in an increased NH_3 adsorption capacity. In this case, the introduction of new surface groups creates more adsorption centres for ammonia than blocking existing ones.

The influence of the surface modification on catalysis

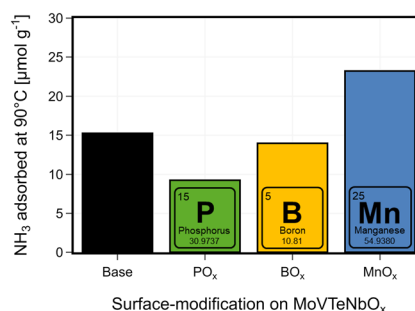All samples were tested in the oxidation of ethane, propane, and n-butane. The base mixed metal oxide $MoVTeNbO_x$

Fig. 6 Quantification of adsorbed ammonia in the NH_3-pulsing study: total amount of NH_3 adsorbed on the base and surface-modified (BO_x–, PO_x–, MnO_x–) $MoVTeNbO_x$ catalyst before catalysis. The samples were dried at 150 °C under He flow for 1 h; 20 NH_3-pulses were performed until saturation of the samples at 90 °C; the overall amount of NH_3 adsorbed is calculated from the differences between the first 15 pulses and the mean signal of saturation (peaks 16–20); see Fig. SI18† for more detail.
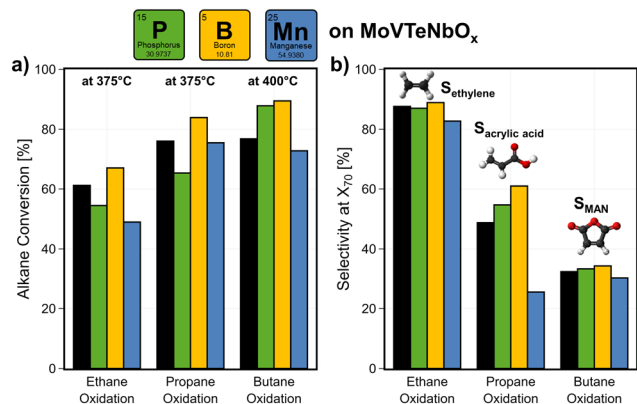
4122 | Catal. Sci. Technol., 2023, **13**, 4117–4130

This journal is © The Royal Society of Chemistry 2023

Fig. 7 Impact of surface modification with BO_x, PO_x, MnO_x on the catalyst performance of MoVTeNbO$_x$: (a) change in alkane conversion at a fixed temperature setpoint of 375 and 400 °C and (b) target-product selectivity (C_2: ethylene, C_3: AA, C_4: MAN) at a fixed conversion level of X_{alkane} = 70% (interpolated) in ethane, propane, and n-butane oxidation. $C_2H_6/O_2/H_2O$ = 3/9/0 % vol, $C_3H_8/O_2/H_2O$ = 3/9/20 % vol, $C_4H_{10}/O_2/H_2O$ = 2/20/3 % vol, 1 atm, 1000 h^{-1} (C_2, C_3), 2000 h^{-1} (C_4).

shows high product yields in all the three reactions, forming ethylene, AA, or MAN from the respective alkane. At 375 °C, alkane conversions of >50% can be achieved on the unmodified catalyst (see Fig. 7a; see Fig. SI19a† for exemplary error bars). Fig. 7b shows the effect on the selectivity towards the desired products at a fixed interpolated conversion level of X_{alkane} = 70%.

BO_x increases both activity and selectivity over MoVTeNbO$_x$ in all three reactions. As MoVTeNbO$_x$ already shows very high ethylene selectivity of $S_{ethylene}$ > 80%, a surface modification with BO_x shows a small improvement. Together with the increased activity, the yield is improved by 7%. Especially in propane oxidation a boost in conversion is achieved, as the conversion is increased from $X_{propane}$ = 76% to 84% at 375 °C (see Fig. SI19b† for change in alkane consumption rates). The selectivity to AA increases by 25% at a fixed conversion. Thus, the overall yield is improved by up to 24% in the selective oxidation of propane at a fixed temperature of 375 °C. Slight improvements of the selectivity towards MAN are achieved in n-butane oxidation. However, BO_x disappears from the near-surface of the catalyst under reaction conditions (Fig. SI14†). This behaviour is similar to what is observed in the industrially used method for moderating temperature profiles within catalyst beds of VPP, in which a volatile phosphorus compound is dosed during operation.[5,103] The deposition of BO_x changes the surface composition of MoVTeNbO$_x$, but partly migrates into its bulk (see Fig. 4b). With that a blocking of active sites cannot be observed in the performance data, while additionally the modified surface (*e.g.* change in electronic properties of V, surface-acidity) helps to desorb the formed products leading to higher selectivity. Furthermore, an increased TOF of all three alkanes seems to be induced by the deposition of BO_x (Fig. SI19c†). Similarly, the incorporation of Nb and Te into

the Mo- and V-based oxide structure significantly improves the catalytic performance and lowers the potential for C–C bond cleavage in all reactions (see Fig. 2). In literature, this effect is attributed to the changing surface compositions under reaction conditions.[19,73] Therefore, an enrichment of Te leads to a reduced abundance of V^{5+}, while on MoVO$_x$ a strong surface-enrichment with V is observed. Thus, the improved performance of BO_x-modified MoVTeNbO$_x$ is attributed to the lowered availability of V on the surface.[19]

The introduction of PO_x lowers the catalytic activity of MoVTeNbO$_x$ in ethane and propane oxidation, but shows a beneficial effect in n-butane oxidation. A slight increase in product selectivity is observed in propane and n-butane oxidation. This effect could be attributed to the blocking of active, but also unselective sites on the surface. Calculated turn over frequencies (TOFs) of the respective alkane (see Fig. SI19b†) show that PO_x deposition has either no or even a positive effect on the alkane consumption rate normalized to V available on the surface.

In contrast to this, the presence of MnO_x leads either to a small decrease (C_2, C_4) or a drop in the selectivity to AA in propane oxidation. In this case, the catalyst is not only less active, but also unselective sites are introduced into the system. This observation is in agreement with the catalytic performance of the perovskite SmMnO$_3$ comprising Mn as redox active element, mostly forming CO_2 from the feedstock. Thus, the addition of MnO_x to the surface of MoVTeNbO$_x$ appears to promote the consecutive combustion of the formed products to CO_x.

In summary, the surface modification of MoVTeNbO$_x$ has both positive and negative effects on the catalytic performance. The analysis of the spent samples shows that the surface deposition of elements does not prevent the surface from adapting to the reaction feed and therefore from restructuring. A comparison before and after catalysis by ICP-OES and XPS indicates a drastic loss in both P and B during the whole catalytic study with >160 h time on stream (see Fig. SI14 and SI15†). This behaviour is known for phosphorus in VPO catalysts, where a loss in surface phosphorus leads to an activation of the catalyst under reaction condition and a change in the V:P ratio.[5,76,103] Nonetheless, a formation of the samples or a change in performance during the study could not be observed, after the samples were exposed to the maximum reaction temperature. The demonstrated tuned performance by the surface modification is therefore maintained and does not follow the loss of the ALD-elements. Additionally, the impact on the surface properties like the oxidation state of V by the surface-modification is still present after the reaction (Fig. 5). While the surface of the base catalyst MoVTeNbO$_x$ is noticeably reduced after catalysis, the XPS spectra of the spent PO_x- and BO_x-modified samples reveal an enrichment of V^{5+} in the near-surface region. Recently, a doping study on MoVTeNbO$_x$ with Bi showed a similar effect of increased AA selectivity, which was correlated to a more oxidized surface state and also an increased Lewis acidity.[104] In contrast, the MnO_x-modified sample shows an even more reduced oxidation state of V

This journal is © The Royal Society of Chemistry 2023

Catal. Sci. Technol., 2023, **13**, 4117–4130 | **4123**

compared to the base catalyst, which is maintained after reaction. Thus, the low AA selectivity measured on this catalyst is consistent with the discussion above. Therefore, a certain flexibility of V at the near-surface appears to be another factor that determines selective oxidation.[105]

Apart from the selected example MoVTeNbO$_x$, the effect of the surface modification on the catalytic performance is investigated systematically for MoVO$_x$, VPP, V$_2$O$_5$, MoO$_3$, and SmMnO$_3$ (Fig. SI20–SI24†). In previous studies V$_2$O$_5$ was used as a model catalyst to study the role of P in VPO-catalysts.[52] A promoting effect was found in n-butane oxidation, which is confirmed for the oxidation of C$_2$ and C$_3$ in the present study. In all reactions, the formation of CO$_x$ is reduced, leading to higher product selectivity. In particular, the PO$_x$-deposition in sub-monolayers (1 ALD-cycle) also leads to an improved catalytic activity. The BO$_x$-modification, however, does not lead to significant improvements on V$_2$O$_5$ (see Fig. SI22†). On the other hand, the deposition of PO$_x$ or BO$_x$, has a beneficial effect on activity and selectivity in some cases, especially for catalysts that already show certain performance in the reactions under investigation (VPP, MoVO$_x$). At the same time, the surface deposition of MnO$_x$ in most cases leads to a reduced performance in partial oxidations. An exception to this trend is MoO$_3$, which shows very low capability to activate the three alkane feedstocks. Here, the surface modification with BO$_x$ or MnO$_x$ leads to slightly elevated alkane conversions and improved selectivity. Especially, the deposited sub-monolayer of MnO$_x$ on MoO$_3$ promotes the oxidative dehydrogenation of propane and a selectivity above 50% is observed (see Fig. SI23†). This result reveals parallels with a study on MnWO$_4$,[106] in which an isolation of MnO$_x$-species on the surface resulted in

improved performance.[89] However, the Mn-based perovskite catalyst acts like a total combustion catalyst forming mostly CO$_2$. Here, the selectivity cannot be tuned by the surface-modification, while a surface-enrichment with Mn clearly leads to a higher catalytic activity.

In addition to temperature, the contact time was varied in catalytic testing. The temperature during this study is fixed to achieve a medium conversion of the base catalysts, while the modified samples are tested under the same conditions. Based on this data, an overview of the different effects of the surface modification is shown in Fig. SI25.† The CO$_x$ formation is often promoted by the deposition of MnO$_x$ e.g., on catalysts, that already show high selectivity (e.g. VPP in C$_4$-oxidation, see Fig. SI26†). While a surface-enrichment of PO$_x$ on the studied phosphate catalyst (VPP), shows no significant change, the addition of PO$_x$ on V$_2$O$_5$, MoVO$_x$, and MoVTeNbO$_x$ leads to an improvement in product selectivity (Fig. 8). Apparently, the interaction between the V-containing bulk and well dispersed PO$_x$ species on the surface of the catalyst reduces the total oxidation of the reactants. It seems that unselective V-sites at the surface are blocked, which in case of MoVTeNbO$_x$ leads to an increased concentration of oxidized V-species in the near-surface region compared to the unmodified catalyst (Fig. 5). Furthermore, the PO$_x$ modification reduces the surface acidity, which could be the reason for the lower activity and the increased selectivity. On the contrary, the deposition of PO$_x$ on the surface of catalysts with another redox active bulk element than V shows no beneficial effect. In comparison, the deposition of BO$_x$ promotes the selectivity in partial oxidations only on specific base catalysts like MoVTeNbO$_x$, while it shows only minor effects on other materials. The mobility of the deposited
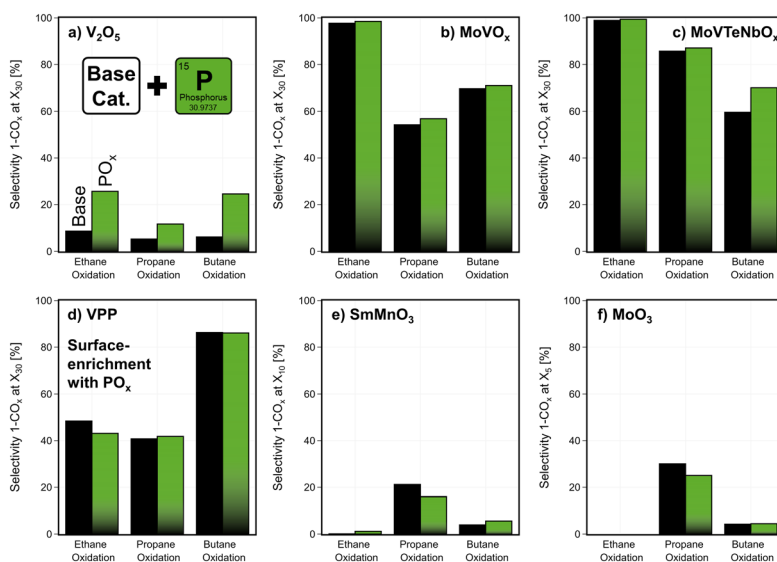

Fig. 8 Change in product formation by the deposition of PO$_x$ on the surface of the six studied catalysts (a) V$_2$O$_5$, (b) MoVO$_x$, (c) MoVTeNbO$_x$, (d) VPP, (e) SmMnO$_3$, (f) MoO$_3$: selectivity towards the sum of partial oxidation products (1-CO$_x$) shown in ethane, propane, n-butane oxidation at fixed temperature setpoint for each reaction and catalyst (see contact time variation study Fig. SI5 and SI6†); the product selectivity is shown at a fixed alkane conversion level by varying the contact time in a range of 500–5000 h^{-1}; the complete contact time variation study can be found in the data set provided in the ESI.† C$_2$H$_6$/O$_2$/H$_2$O = 3/9/0 % vol, C$_3$H$_8$/O$_2$/H$_2$O = 3/9/20 % vol, C$_4$H$_{10}$/O$_2$/H$_2$O = 2/20/3 % vol, 1 atm.

4124 | *Catal. Sci. Technol.*, 2023, **13**, 4117–4130

This journal is © The Royal Society of Chemistry 2023

species and consecutively the migration to the bulk of catalysts, as shown for BO_x–$MoVTeNbO_x$, could be the reason for only slight changes in performance on catalysts like V_2O_5 or $MoVO_x$ (see Fig. SI27†). In contrast to this, in case of $MoVTeNbO_x$ the most notable improvements are achieved by the BO_x-modification. The fact that this catalyst is already very selective in the studied reactions might play a role here, as the element deposition could also lead to blocking of active sites. Therefore, with the addition of BO_x on the surface most of the features of the base catalyst are sustained, while surface properties can be tuned. In summary, the surface modification by ALD enables an optimized potential of the catalysts to partially oxidize the alkane feedstocks, as shown Fig. 8.

According to these results the surface modification has both beneficial and unfavourable effects on selectivity, depending on the catalyst and the reaction. However, the overall product distribution (see Fig. 2) can only be adjusted without completely changing in selectivity. One reason for this is the deposition of only one ALD-cycle on the catalysts, which correspond to a sub-monolayer.[53] In previous studies it could be shown that the deposition of multiple cycles can intensify the observed effects.[52] Beyond a certain amount of precursor deposited on the surface of the catalyst, however, the formation of new (crystalline-) phases is possible. With the deposition of one ALD-cycle resulting in a homogeneous dispersion, the effect of oxide species (PO_x, BO_x, MnO_x) as promotors is studied rather than forming new active phases on the surface. On the other hand, the catalytic performance of the samples modified with a sub-monolayer is still dominated by the properties of the base catalyst. Furthermore, the catalyst surfaces still undergo a restructuring process, when exposed to the reaction feeds, as shown by the comparison of fresh and spent samples (see Fig. SI15 and SI17†). Therefore, the formation of the actual active surface layer is supported by stable bulk characteristics. This is in line with the fact that the bulk has an important function in catalysis,[107,108] while most of the elemental steps of the actual reaction are proceeding at the termination layer. As a result, in particular the interplay between the bulk and the dynamic surface of a bulk catalyst seems to be the key for high performance in selective oxidation reactions.[41,42,109]

Conclusion

An efficient selective oxidation of different alkanes requires catalysts with the ability to activate the feedstock while the total oxidation of the products or intermediates by parallel or consecutive reactions is suppressed. The best performance with high yields of the desired products (MAN, AA, ethylene) is achieved by catalysts from two different families, namely the mixed metal oxide $MoVTeNbO_x$, and the vanadium phosphate VPP. A common feature of both materials is the formation of a surface layer under reaction conditions, that significantly differs from its bulk. The surface modification

with the promoting elements PO_x, BO_x, and MnO_x is used to tune the catalytic properties of oxidation catalysts. A homogeneous element dispersion on the surface is ensured by the utilization of ALD, while maintaining the mechanical properties of the base catalysts. The deposition of PO_x on V-based oxides is demonstrated to enhance the oxygenate or olefin formation in alkane oxidation. Similarly, BO_x could be identified as another promotor of the studied reactions, resulting in increased product selectivity and catalytic activity. The systematic study of six base catalyst with three deposition-elements revealed a broad range of effects, of which certain modified surface properties can be attributed to improved performance. In case of the mixed metal oxide $MoVTeNbO_x$, the deposition of PO_x and BO_x yields in an increase in productivity of up to 24%, for instance in the oxidation of propane to AA. In this case, XPS studies reveal that the beneficial effect in catalysis is connected to an oxidized surface state with the accumulation of V^{5+} in the near-surface region. Furthermore, a reduced acidity is shown to be another common characteristic of the surface modification of $MoVTeNbO_x$ with PO_x and BO_x. On the other hand, the deposition of another redox element like Mn induces a reduction of the V-species on the surface and furthermore to additional acidic sites. These changes in surface properties come along with an increased formation of CO_x and a reduction in catalytic activity. However, the introduction of Mn to a mostly inert oxide like MoO_3 or an enrichment of Mn on the $SmMnO_3$ perovskite shows an increase in performance. The elements are deposited as partial monolayers by ALD on the oxidation catalysts without changing their basic features. Thus, the change in surface-properties like the acidity or the surface state of the termination groups shows a good agreement with the observed change in performance. This study, including 18 combinations of base catalysts and promoting elements studied in three reactions, suggests that the catalytic performance of a bulk catalyst is tuneable by varying its surface properties with synthetic means. Here, it is crucial to preserve the important bulk properties of the catalysts by using solvent free techniques like ALD. This method proves to be a powerful tool for precise addition of promotor compounds to bulk catalysts. Based on this study, the product formation of V-containing oxide catalysts can be tuned by the introduction of finely dispersed PO_x. For future applications, the deposition of more than one sub-monolayer of potentially beneficial elements in multiple ALD-cycles could further enhance product formation. Additionally, a variety of different elements can be deposited by ALD, potentially leading to further improved catalytic performance.

Experimental section

Base catalysts

Six bulk oxidation catalysts are selected from a collection of oxides or phosphates with a well-known catalytic activity in selective oxidations.[38] A preferably broad range of catalytic

This journal is © The Royal Society of Chemistry 2023

Catal. Sci. Technol., 2023, **13**, 4117–4130 | **4125**

behaviours is covered with highly active and less active catalysts, full combustion catalysts, and very selective catalysts. First, binary or monometallic oxides comprising the most commonly used elements in selective oxidation reactions are included, namely V_2O_5 and MoO_3. The combination of both elements as multi-metal oxides with M1 structure type, represented by $MoVO_x$ and $MoVTeNbO_x$, enables improved activity in the respective reactions. While the state-of-the-art performance in C_2 and C_3 oxidation can be achieved by these metal oxide catalysts, for an efficient n-butane oxidation to MAN especially VPO catalysts, like VPP, are used. Finally, the perovskite catalyst $SmMnO_3$ is selected, which could be shown to activate C–H bonds very efficiently but shows rather low selectivity in partial oxidation reactions. The bulk catalysts were prepared in sufficient batch size (20 g) and as phase pure samples, according to synthesis-protocols, that are described in detail elsewhere.[40] Linked references are listed in the ESI,† from which the synthesis protocols are adapted. The samples are pressed (1 t, 1 min, d_{pellet} = 14 mm), crushed, and sieved to a particle size fraction of 100–200 μm, for both the performance studies and the surface modification.

Atomic layer deposition

Sub-monolayers of phosphorus-, boron-, and manganese-oxide are deposited on the surface of the base catalysts using atomic layer deposition (ALD).[44–46,50] During the first ALD half cycle, the gaseous precursors of the respective element P (tris-(dimethylamino)-phosphate, DMAP, Sigma-Aldrich, 97%), B (trimethylborate, TMB, Sigma-Aldrich, ≥98%), Mn (bis(ethyl-cyclopentadienyl)manganese, MnCpEt, Strem, ≥98%) diluted with argon (99.999%) is introduced in a quartz tube fixed bed reactor containing 5 ml of the catalyst until saturation of the surface sites (100 ml min⁻¹, 1 atm) is achieved. The reactor is heated to 70 °C for the deposition of the phosphorus precursor and 150 °C in the case of boron and manganese. The precursor dosing units were kept at 25 °C (DMA, TMB) or 100 °C (MnCpEt). The point of precursor or reactant saturation was determined by online mass spectrometry. The mass gain or ALD growth during the whole process is monitored by an *in situ* magnetic suspension balance[44] (see example in Fig. SI13†). In the second half cycle, water or oxygen is used as a reactant to remove the ligands, leaving the surface with PO_x and BO_x, or MnO_x-groups, respectively. In between, before and after the half-cycles the sample is purged with argon. Details about the experimental setup and the ALD process are described elsewhere.[47,53] In this study one ALD-cycle is applied to the catalysts, which yields in sub-monolayers of the elements on the catalysts. After a fixed pre-treatment in dry synthetic air (20% O_2 in N_2) at 275 °C (mixed metal oxides) or 450 °C for 4 h, the modified samples are cooled down and sieved for catalyst testing.

Catalyst testing

Base catalysts and modified samples are studied in the selective oxidation of short-chain alkanes (n-butane, propane,

ethane). The feed composition is fixed based on industrial or academic standards (C_4-oxidation,[24] C_3-oxidation[11]) balanced by nitrogen ($C_4H_{10}/O_2/H_2O$: 2/20/3; $C_3H_8/O_2/H_2O$: 3/9/20; $C_2H_6/O_2/H_2O$: 3/9/0 % vol) at a gas hourly space velocity (GHSV) of 2000 h⁻¹ (C_4) or 1000 h⁻¹ (C_2, C_3) and atmospheric pressure. The performance studies are performed in commercial parallel test setups (hte GmbH, ILS GmbH) with sample volumes of V = 0.7/1.0 ml in stainless steel reactors with a diameter of d = 7/10 mm. The reaction temperature is individually controlled in the range of 225 to 450 °C, while an alkane or oxygen conversion of X_{alkane} = 85% must not be exceeded. Outlet concentrations are monitored using an online gas chromatography system. Argon is used as an internal standard to eliminate possible gas expansion in the calculation of conversion and selectivity and a blank reactor is used for online measurements of the input gas feed. More details on the technical setup and the evidence of independence of mass and heat transfer limitations are described elsewhere.[9,110]

The design of experiments (DoE) is fixed for all tested samples and includes a temperature and GHSV variation study. The reaction temperature is gradually increased in 25 K steps until 450 °C max or until a reactant conversion X_{alkane} < 85% is achieved. After the temperature is decreased again, it is fixed to a setpoint of about X_{alkane} = 15%. The GHSV is varied at four different setpoints (500 to 5000 h⁻¹). Raw-data evaluation was performed using the commercial software tool myhte™. The calculation of the presented performance parameters (X, S) is done product-based (see eqn (4)–(8)); the whole set of raw data, can be found in the ESI.†

$$X_{alkane} \, [\%] = 1 - \frac{\sum c_{products}}{\sum (c_{alkane} + c_{products})} \cdot \frac{c_{Ar,0}}{c_{Ar}} \quad (4)$$

$$S_i \, [\%] = \frac{c_i \cdot c_{Ar,0}}{\sum (c_{alkane} + c_{products}) \cdot c_{Ar} - c_{alkane} \cdot c_{Ar,0}} \cdot \frac{N_{c,i}}{N_{c\text{-}alkane}} \quad (5)$$

$$r_{alkane} \, [\text{mmol g}^{-1} \text{h}^{-1}] = \frac{\frac{X_{alkane} \cdot c_{0,alkane} \cdot \dot{V}_{Feed}}{V_m} \cdot 1000}{m_{cat}} \cdot \frac{c_{Ar,0}}{c_{Ar}} \quad (6)$$

$$r_{alkane} \, [\text{mmol m}^{-2} \text{h}^{-1}] = \frac{r_{alkane} \, [\text{mmol g}^{-1} \text{h}^{-1}]}{\text{BET surf. area } [\text{m}^2 \text{g}^{-1}]} \quad (7)$$

$$r_i \, [\text{mmol g}^{-1} \text{h}^{-1}] = r_{alkane} \, [\text{mmol g}^{-1} \text{h}^{-1}] \cdot S_i \quad (8)$$

Characterization

N₂-physisorption. Nitrogen sorption analysis was performed at 77 K (liquid N_2) using a Quadrasorb SI device manufactured by Quantachrome. The samples were degassed at ϑ = 200 °C for 2 h ahead of the measurements. The surface area was determined by the Brunauer–Emmett–Teller (BET) method in the linear P/P_0 = 0.05–0.3 pressure range of selected fresh, spent, base and surface-modified catalysts. The pore size distribution is calculated based on the N_2-desorption using the BJH-method.

4126 | *Catal. Sci. Technol.*, 2023, **13**, 4117–4130

This journal is © The Royal Society of Chemistry 2023

X-ray diffraction. X-ray powder diffraction (XRPD) patterns were recorded at ambient temperature using an X'PERT Pro manufactured by PANalytical equipped with a scintillation detector (Cu Kα1 radiation, λ = 0.154 nm, 15 minutes exposure time in the angular range $10° \leq 2\theta < 80°$). XRPD is used to monitor possible changes in the crystal structure of the bulk catalysts during the surface modification or catalytic studies.

Elemental analysis. X-ray photoelectron spectroscopy (XPS) was carried out using a Thermo Fisher Scientific K-Alpha. A monochromatic Al-Kα X-ray source (1486.6 eV) was employed for the analysis, using a spot size of 200 microns, a pass energy of 200 eV for a survey, and 50 eV for high-resolution spectra. The samples were mounted on conductive carbon tape. The analysis of the spectra was done using the Avantage software with Shirley background and a Gaussian–Lorentzian ratio of 30% for the peak deconvolution. The C1s peak of adventitious carbon at 284.8 eV was taken as a reference for charge-shift correction for the measured spectra. For deconvolution of the V^{4+}/V^{5+} species, only the V $2p_{3/2}$ region is used as the V $2p_{1/2}$ overlaps with an O1s satellite, in addition to the low V content of the samples (see Fig. SI16†). The ratio R_{XPS} between both oxidation states was calculated according to eqn (9). No further oxidation states of V species were detected.

$$R_{XPS} = \frac{V^{4+}}{(V^{4+} + V^{5+})} \tag{9}$$

Further details on the evaluation of the XPS spectra (Mo, Te, Nb, P, B, Mn) can be found in Fig. SI16.†[12,18,53] Inductively coupled plasma optical emission spectrometry (ICP-OES) was conducted for the elemental analysis (Mo, V, Te, Nb, B, P) of the bulk composition by the contract laboratory Mikroanalytisches Labor Kolbe, Oberhausen (Germany).

Scanning transmission electron microscopy. STEM was performed on a FEI Talos F200X (Thermo Fisher Scientific, Waltham MA, USA) with an XFEG field emission gun and acceleration voltage of 200 kV. Energy-dispersive X-ray (EDX) mappings were recorded with a SuperX system of four SDD EDX detectors (Analysis software: Velox 2.9.0 by Thermo Fisher Scientific).

Adsorption of ammonia. NH$_3$-adsorption measurements are conducted using an AMI-300 equipped with thermal conductivity detector (TCD) from Altamira Instrument. Around 0.05 g of catalyst sample (with a particle size fraction of 100–200 μm) is placed in the measurement cell (quartz U-tube) and is fixed in place by quartz wool. The measurements are initiated by a drying or pre-treatment step at 150 °C in He flow for 1 h. Then, 20 pulses with a fixed amount of NH$_3$ diluted in He (40% NH$_3$ in He) are dosed at 90 °C, while the adsorption is monitored by TCD. The number of pulses is selected to achieve a complete saturation of the catalyst powder. The amount of adsorbed NH$_3$ is calculated based on the difference between the peak integral before saturation (pulse 1 to 15) and the mean integral of the peaks at saturation (pulse 16 to 20) of the sample. The results are corrected by a reference measurement without sample (weighted wool and empty quartz tube) under the same conditions.

Author contributions

The manuscript was written through contributions of all authors. All authors have given approval to the final version of the manuscript.

Conflicts of interest

The authors declare no conflict of interest.

Acknowledgements

References

1 *Research needs towards sustainable production of fuels and chemicals*, ed. J. K. Nørskov, A. Latimer and C. F. Dickens, 2019, Accessed Nov. 2022.

2 P. T. Anastas, M. M. Kirchhoff and T. C. Williamson, *Appl. Catal., A*, 2001, **221**, 3–13.

3 G. Centi and S. Perathoner, *Catal. Today*, 2003, **77**, 287–297.

4 F. Cavani and J. H. Teles, *ChemSusChem*, 2009, **2**, 508–534.

5 G. Mestl, D. Lesser and T. Turek, *Top. Catal.*, 2016, **59**, 1533–1544.

6 N. Ballarini, F. Cavani, C. Cortelli, S. Ligi, F. Pierelli, F. Trifirò, C. Fumagalli, G. Mazzoni and T. Monti, *Top. Catal.*, 2006, **38**, 147–156.

7 F. Trifirò and R. K. Grasselli, *Top. Catal.*, 2014, **57**, 1188–1195.

8 N. F. Dummer, J. K. Bartley and G. J. Hutchings, *Adv. Catal.*, 2011, **54**, 189–247.

9 C. Schulz, F. Pohl, M. Driess, R. Glaum, F. Rosowski and B. Frank, *Ind. Eng. Chem. Res.*, 2019, **58**, 2492–2502.

10 G. Mestl, J. L. Margitfalvi, L. Végvári, G. P. Szijjártó and A. Tompos, *Appl. Catal., A*, 2014, **474**, 3–9.

11 R. Naumann d'Alnoncourt, L. I. Csepei, M. Hävecker, F. Girgsdies, M. E. Schuster, R. Schlögl and A. Trunschke, *J. Catal.*, 2014, **311**, 369–385.

12 M. Hävecker, S. Wrabetz, J. Kröhnert, L. I. Csepei, R. Naumann d'Alnoncourt, Y. V. Kolen'Ko, F. Girgsdies, R. Schlögl and A. Trunschke, *J. Catal.*, 2012, **285**, 48–60.

This journal is © The Royal Society of Chemistry 2023

Catal. Sci. Technol., 2023, **13**, 4117–4130 | **4127**

13 R. Schlögl, *Top. Catal.*, 2011, **54**, 627–638.

14 D. Melzer, G. Mestl, K. Wanninger, A. Jentys, M. Sanchez-Sanchez and J. A. Lercher, *Top. Catal.*, 2020, **63**, 1754–1764.

15 D. Melzer, G. Mestl, K. Wanninger, Y. Zhu, N. D. Browning, M. Sanchez-Sanchez and J. A. Lercher, *Nat. Commun.*, 2019, **10**, 4012.

16 K. F. Kalz, R. Kraehnert, M. Dvoyashkin, R. Dittmeyer, R. Gläser, U. Krewer, K. Reuter and J. D. Grunwaldt, *ChemCatChem*, 2017, **9**, 17–29.

17 J. C. Volta, *Catal. Today*, 1996, **32**, 29–36.

18 A. C. Sanfiz, T. W. Hansen, D. Teschner, P. Schnörch, F. Girgsdies, A. Trunschke, R. Schlögl, M. H. Looi and S. B. Abd Hamid, *J. Phys. Chem. C*, 2010, **114**, 1912–1921.

19 A. Trunschke, J. Noack, S. Trojanov, F. Girgsdies, T. Lunkenbein, V. Pfeifer, M. Hävecker, P. Kube, C. Sprung, F. Rosowski and R. Schlögl, *ACS Catal.*, 2017, **7**, 3061–3071.

20 R. Schlögl, *Angew. Chem., Int. Ed.*, 2015, **54**, 3465–3520.

21 T. Zambelli, J. Wintterlin, J. Trost and G. Ertl, *Science*, 1996, **273**, 1688–1690.

22 G. A. Somorjai, *Langmuir*, 1991, **7**, 3176–3182.

23 G. Ertl, *Angew. Chem.*, 1990, **102**, 1258–1266.

24 C. Schulz, R. Kraehnert, F. Rosowski and B. Frank, *ChemCatChem*, 2018, **10**, 5523–5532.

25 E. W. Arnold and S. Sundaresan, *Chem. Eng. Commun.*, 2007, **58**, 213–230.

26 C. Heine, M. Hävecker, E. Stotz, F. Rosowski, A. Knop-Gericke, A. Trunschke, M. Eichelbaum and R. Schlögl, *J. Phys. Chem. C*, 2014, **118**, 20405–20412.

27 M. Eichelbaum, M. Hävecker, C. Heine, A. Karpov, C.-K. Dobner, F. Rosowski, A. Trunschke and R. Schlögl, *Angew. Chem., Int. Ed.*, 2012, **51**, 6246–6250.

28 M. A. Carreon and V. V. Guliants, *Catal. Today*, 2003, **78**, 303–310.

29 M. Abon, K. E. Bere, A. Tuel and P. Delichere, *J. Catal.*, 1995, **156**, 28–36.

30 G. Busca and G. Centi, *J. Am. Chem. Soc.*, 1989, **111**, 46–54.

31 F. Ben Abdelouahab, R. Olier, N. Guilhaume, F. Lefebvre and J. C. Volta, *J. Catal.*, 1992, **134**, 151–167.

32 E. A. Mamedov, *Appl. Catal., A*, 1994, **116**, 49–70.

33 V. V. Guliants, R. Bhandari, B. Swaminathan, V. K. Vasudevan, H. H. Brongersma, A. Knoester, A. M. Gaffney and S. Han, *J. Phys. Chem. B*, 2005, **109**(50), 24046–24055.

34 V. V. Guliants, H. H. Brongersma, A. Knoester, A. M. Gaffney and S. Han, *Top. Catal.*, 2006, **38**, 41–50.

35 T. V. Andrushkevich and E. V. Ovchinnikova, *Mol. Catal.*, 2020, **484**, 110734.

36 C. Heine, M. Hävecker, A. Trunschke, R. Schlögl and M. Eichelbaum, *Phys. Chem. Chem. Phys.*, 2015, **17**, 8983–8993.

37 A. Trunschke, *Catal. Sci. Technol.*, 2022, **12**, 3650–3669.

38 A. Trunschke, G. Bellini, M. Boniface, S. J. Carey, J. Dong, E. Erdem, L. Foppa, W. Frandsen, M. Geske, L. M. Ghiringhelli, F. Girgsdies, R. Hanna, M. Hashagen, M. Hävecker, G. Huff, A. Knop-Gericke, G. Koch, P. Kraus, J. Kröhnert, P. Kube, S. Lohr, T. Lunkenbein, L. Masliuk, R. Naumann d'Alnoncourt, T. Omojola, C. Pratsch, S. Richter, C. Rohner, F. Rosowski, F. Rüther, M. Scheffler, R. Schlögl, A. Tarasov, D. Teschner, O. Timpe, P. Trunschke, Y. Wang and S. Wrabetz, *Top. Catal.*, 2020, **63**, 1683–1699.

39 L. Foppa, L. M. Ghiringhelli, F. Girgsdies, M. Hashagen, P. Kube, M. Hävecker, S. J. Carey, A. Tarasov, P. Kraus, F. Rosowski, R. Schlögl, A. Trunschke and M. Scheffler, *MRS Bull.*, 2021, **46**, 1016–1026.

40 L. Foppa, F. Rüther, M. Geske, G. Koch, F. Girgsdies, P. Kube, S. Carey, M. Hävecker, O. Timpe, A. Tarasov, M. Scheffler, F. Rosowski, R. Schlögl and A. Trunschke, *J. Am. Chem. Soc.*, 2023, **145**(6), 3427–3442.

41 S. V. Merzlikin, N. N. Tolkachev, L. E. Briand, T. Strunskus, C. Wöll, I. E. Wachs, W. Grünert, S. V. Merzlikin, W. Grünert, N. N. Tolkachev, N. D. Zelinsky, L. E. Briand, T. Strunskus and C. Wöll, *Angew. Chem., Int. Ed.*, 2010, **49**, 8037–8041.

42 R. Schlögl, *Top. Catal.*, 2016, **59**, 1461–1476.

43 M. Eichelbaum, M. Hävecker, C. Heine, A. M. Wernbacher, F. Rosowski, A. Trunschke and R. Schlögl, *Angew. Chem., Int. Ed.*, 2015, **54**, 2922–2926.

44 J. Lu, J. W. Elam and P. C. Stair, *Surf. Sci. Rep.*, 2016, **71**, 410–472.

45 B. J. Oneill, D. H. K. Jackson, J. Lee, C. Canlas, P. C. Stair, C. L. Marshall, J. W. Elam, T. F. Kuech, J. A. Dumesic and G. W. Huber, *ACS Catal.*, 2015, **5**, 1804–1825.

46 H. Zhang and C. L. Marshall, *Chin. J. Catal.*, 2019, **40**, 1311–1323.

47 V. E. Strempel, R. Naumann D'Alnoncourt, M. Driess and F. Rosowski, *Rev. Sci. Instrum.*, 2017, **88**, 74102.

48 K. Knemeyer, R. Baumgarten, P. Ingale, R. Naumann D'Alnoncourt, M. Driess and F. Rosowski, *Rev. Sci. Instrum.*, 2021, **92**, 25115.

49 R. Baumgarten, P. Ingale, K. Knemeyer, R. Naumann d'Alnoncourt, M. Driess and F. Rosowski, *Nanomaterials*, 2022, **12**, 1458.

50 V. Miikkulainen, M. Leskelä, M. Ritala and R. L. Puurunen, *J. Appl. Phys.*, 2013, **113**, 021301.

51 V. E. Strempel, D. Löffler, J. Kröhnert, K. Skorupska, B. Johnson, R. Naumann d'Alnoncourt, M. Driess and F. Rosowski, *J. Vac. Sci. Technol., A*, 2015, **34**, 01A135.

52 K. Knemeyer, J. D. Epping, F. Rüther, C. Schulz, B. Frank, P. Müller, R. Naumann d'Alnoncourt, M. Driess and F. Rosowski, *ChemCatChem*, 2021, **13**, 4201.

53 K. Knemeyer, M. P. Hermida, P. Ingale, J. Schmidt, J. Kröhnert, R. Naumann d'Alnoncourt, M. Driess and F. Rosowski, *Phys. Chem. Chem. Phys.*, 2020, **22**, 17999–18006.

54 P. Ingale, K. Knemeyer, P. Preikschas, M. Ye, M. Geske, R. Naumann d'Alnoncourt, A. Thomas and F. Rosowski, *Catal. Sci. Technol.*, 2021, **11**, 484–493.

55 P. Ingale, K. Knemeyer, M. P. Hermida, R. Naumann d'Alnoncourt, A. Thomas and F. Rosowski, *Nanomaterials*, 2020, **10**, 981.

56 R. Baumgarten, R. Naumann d'Alnoncourt, S. Lohr, E. Gioria, E. Frei, E. Fako, S. De, C. Boscagli, M. Drieß, S. Schunk and F. Rosowski, *Chem. Ing. Tech.*, 2022, **94**, 1765–1775.

57 S. T. Oyama and G. A. Somorjai, *J. Phys. Chem.*, 1990, **94**, 5022–5028.

4128 | *Catal. Sci. Technol.*, 2023, **13**, 4117–4130

This journal is © The Royal Society of Chemistry 2023

58 T. Ressler, J. Wienold, R. E. Jentoft and F. Girgsdies, *Eur. J. Inorg. Chem.*, 2003, **2003**, 301–312.

59 C.-C. Liao, C.-C. Chang, Y. M. Choi and M.-K. Tsai, *Surf. Sci.*, 2018, **674**, 45–50.

60 T. Katou, D. Vitry and W. Ueda, *Catal. Today*, 2004, **91–92**, 237–240.

61 W. Ueda, D. Vitry and T. Katou, *Catal. Today*, 2005, **99**, 43–49.

62 A. M. Wernbacher, P. Kube, M. Hävecker, R. Schlögl and A. Trunschke, *J. Phys. Chem. C*, 2019, **123**, 13269–13282.

63 J. M. López Nieto, B. Solsona, P. Concepción, F. Ivars, A. Dejoz and M. I. Vázquez, *Catal. Today*, 2010, **157**, 291–296.

64 J. M. López Nieto, P. Botella, M. I. Vázquez and A. Dejoz, *Chem. Commun.*, 2002, 1906–1907.

65 C. Heine, M. Hävecker, M. Sanchez-Sanchez, A. Trunschke, R. Schlögl and M. Eichelbaum, *J. Phys. Chem. C*, 2013, **117**, 26988–26997.

66 G. J. Hutchings, *Catal. Today*, 1993, **16**, 139–146.

67 P. Ciambelli, S. Cimino, S. De Rossi, M. Faticanti, L. Lisi, G. Minelli, I. Pettiti, P. Porta, G. Russo and M. Turco, *Appl. Catal., B*, 2000, **24**, 243–253.

68 G. Koch, M. Hävecker, D. Teschner, S. J. Carey, Y. Wang, P. Kube, W. Hetaba, T. Lunkenbein, G. Auffermann, O. Timpe, F. Rosowski, R. Schlögl and A. Trunschke, *ACS Catal.*, 2020, **10**, 7007–7020.

69 F. Ivars, P. Botella, A. Dejoz, J. M. López Nieto, P. Concepción and M. I. Vázquez, *Top. Catal.*, 2006, **38**, 59–67.

70 J. T. Herron and R. E. Huie, *J. Phys. Chem.*, 1969, **73**, 3327–3337.

71 J. Haber, *Handbook of Heterogeneous Catalysis*, 2008.

72 P. Mars and D. W. van Krevelen, *Chem. Eng. Sci.*, 1954, **3**, 41–59.

73 A. de Arriba, B. Solsona, E. García-González, P. Concepción and J. M. López Nieto, *Appl. Catal., A*, 2022, **643**, 118780.

74 M. Jaber Darabi Mahboub, J. L. Dubois, F. Cavani, M. Rostamizadeh and G. S. Patience, *Chem. Soc. Rev.*, 2018, **47**, 7703–7738.

75 M. J. Cheng and W. A. Goddard, *J. Am. Chem. Soc.*, 2013, **135**, 4600–4603.

76 B. K. Hodnett and B. Delmon, *J. Catal.*, 1984, **88**, 43–53.

77 Y. H. Taufiq-Yap, C. K. Goh, G. J. Hutchings, N. Dummer and J. Bartley, *Catal. Lett.*, 2009, **130**, 327–334.

78 W. C. O'Leary, W. A. Goddard and M. J. Cheng, *J. Phys. Chem. C*, 2017, **121**, 24069–24076.

79 R. K. Grasselli, C. G. Lugmair and A. F. Volpe, *Top. Catal.*, 2008, **50**, 66–73.

80 T. Ushikubo, *Catal. Today*, 2003, **78**, 79–84.

81 O. V. Buyevskaya, D. Müller, I. Pitsch and M. Baerns, in *Natural gas conversion V*, ed. A. Parmaliana, Elsevier, Amsterdam, New York, 1998, pp. 671–676.

82 P. Kube, J. Dong, N. S. Bastardo, H. Ruland, R. Schlögl, J. T. Margraf, K. Reuter and A. Trunschke, *Nat. Commun.*, 2022, **13**, 7504.

83 W. P. McDermott, M. C. Cendejas and I. Hermans, *Top. Catal.*, 2020, **63**, 1700–1707.

84 J. M. Venegas, Z. Zhang, T. O. Agbi, W. P. McDermott, A. Alexandrova and I. Hermans, *Angew. Chem., Int. Ed.*, 2020, **59**, 16527.

85 J. T. Grant, W. P. McDermott, J. M. Venegas, S. P. Burt, J. Micka, S. P. Phivilay, C. A. Carrero and I. Hermans, *ChemCatChem*, 2017, **9**, 3623–3626.

86 J. A. Loiland, Z. Zhao, A. Patel and P. Hazin, *Ind. Eng. Chem. Res.*, 2019, **58**, 2170–2180.

87 P. Kraus and R. P. Lindstedt, *J. Phys. Chem. C*, 2021, **125**, 5623–5634.

88 X. Zhang, R. You, Z. Wei, X. Jiang, J. Yang, Y. Pan, P. Wu, Q. Jia, Z. Bao, L. Bai, M. Jin, B. Sumpter, V. Fung, W. Huang and Z. Wu, *Angew. Chem., Int. Ed.*, 2020, **59**, 8042–8046.

89 X. Li, T. Lunkenbein, V. Pfeifer, M. Jastak, P. K. Nielsen, F. Girgsdies, A. Knop-Gericke, F. Rosowski, R. Schlögl and A. Trunschke, *Angew. Chem., Int. Ed.*, 2016, **55**, 4092–4096.

90 K. Amakawa, Y. Wang, J. Kröhnert, R. Schlögl and A. Trunschke, *Mol. Catal.*, 2019, **478**, 110580.

91 V. V. Guliants, J. B. Benziger, S. Sundaresan and I. E. Wachs, *Stud. Surf. Sci. Catal.*, 2000, **130**, 1721–1726.

92 F. Cavani and F. Trifirò, *Stud. Surf. Sci. Catal.*, 1997, **110**, 19–34.

93 M. Niwa, Y. Habuta, K. Okumura and N. Katada, *Catal. Today*, 2003, **87**, 213–218.

94 Y. Moro-oka, *Appl. Catal., A*, 1999, **181**, 323–329.

95 P. Concepción, P. Botella and J. M. López Nieto, *Appl. Catal., A*, 2004, **278**, 45–56.

96 M. Baca, A. Pigamo, J. L. Dubois and J. Millet, *Catal. Commun.*, 2005, **6**, 215–220.

97 F. Ivars-Barceló, J. Millet, T. Blasco, P. Concepción, J. S. Valente and J. M. López Nieto, *Catal. Today*, 2014, **238**, 41–48.

98 K. Bhaduri, A. Auroux, A. Bhaumik and B. Chowdhury, *Appl. Organomet. Chem.*, 2022, **36**(12), e6904.

99 G. Busca, G. Centi, F. Trifiro and V. Lorenzelli, *J. Phys. Chem.*, 1986, **90**, 1337–1344.

100 A. Stanislaus, M. Absi-Halabi and K. Al-Doloma, *Appl. Catal.*, 1988, **39**, 239–253.

101 D. C. Upham, M. Orazov and T. F. Jaramillo, *J. Catal.*, 2021, **399**, 132–141.

102 T. V. Andrushkevich, G. Y. Popova, Y. A. Chesalov, E. V. Ischenko, M. I. Khramov and V. V. Kaichev, *Appl. Catal., A*, 2015, **506**, 109–117.

103 F. Garbassi, *J. Catal.*, 1986, **98**, 317–325.

104 R. Quintana-Solórzano, I. Mejía-Centeno, H. Armendáriz-Herrera, J. Ramírez-Salgado, A. Rodríguez-Hernandez, M. D. L. Guzmán-Castillo, J. M. López Nieto and J. S. Valente, *ACS Omega*, 2021, **6**, 15279–15291.

105 J. Ramírez-Salgado, R. Quintana-Solórzano, I. Mejía-Centeno, H. Armendáriz-Herrera, A. Rodríguez-Hernández, M. de Lourdes Guzmán-Castillo and J. S. Valente, *Appl. Surf. Sci.*, 2022, **573**, 151428.

106 X. Li, T. Lunkenbein, J. Kröhnert, V. Pfeifer, F. Girgsdies, F. Rosowski, R. Schlögl and A. Trunschke, *Faraday Discuss.*, 2016, **188**, 99–113.

107 C. Zhao and I. E. Wachs, *J. Catal.*, 2008, **257**, 181–189.

108 R. K. Grasselli, *Top. Catal.*, 2002, **21**, 79–88.

This journal is © The Royal Society of Chemistry 2023

Catal. Sci. Technol., 2023, **13**, 4117–4130 | **4129**

109 M. Eichelbaum, R. Glaum, M. Hävecker, K. Wittich, C. Heine, H. Schwarz, C.-K. Dobner, C. Welker-Nieuwoudt, A. Trunschke and R. Schlögl, *ChemCatChem*, 2013, **5**, 2318–2329.

110 C. Schulz, S. C. Roy, K. Wittich, R. Naumann d'Alnoncourt, S. Linke, V. E. Strempel, B. Frank, R. Glaum and F. Rosowski, *Catal. Today*, 2019, **333**, 113–119.

4130 | *Catal. Sci. Technol.*, 2023, **13**, 4117–4130

This journal is © The Royal Society of Chemistry 2023